START-TO-END BEAM DYNAMICS SIMULATIONS FOR THE SRF ACCELERATOR TEST FACILITY AT FERMILAB*

C.R. Prokop [1], P. Piot [1,2], M. Church [2], Y.-E Sun[2]
[1] Department of Physics, Northern Illinois University DeKalb, IL 60115, USA
[2] Fermi National Accelerator Laboratory, Batavia, IL 60510, USA

Abstract

Fermilab is currently building a superconducting RF (SCRF) linear-accelerator test facility. In addition to testing ILC-spec SCRF accelerating modules for ILC and Project-X, the facility will be capable of supporting a variety of advanced accelerator R&D experiments. The accelerator facility includes a 40-MeV photoinjector capable of producing bunches with variable parameters. In this paper, we present start-to-end simulations of the accelerator beamline.

INTRODUCTION

A superconducting test facility (STF) is under construction at Fermilab's New Muon Labotary (NML) building, with first-beam planned for sometime in 2012 [1]. The primary purpose of the facility (referred to as STF@NML in the following) is to develop and explore the operational performance of superconducting accelerating modules for the International Linear Collider (ILC). In addition, the facility will also be a test bed for the relativistic portion of Fermilab's Project-X [2]. The construction of STF@NML will be staged and in its final configuration the facility is expected to produce $\sim$ 900 MeV electron beams capable of supporting advanced accelerator R&D (AARD) experiments.

The STF@NML incorporates a rf photoinjector capable of producing $\sim$ 40-MeV bunches. The beamline layout is shown in Fig. 1. The beam generation and acceleration section includes a 1.3-GHz rf gun, two 1.3-GHz superconducting cavities (CAV1 and CAV2) and, at a later stage, will eventually incorporate a 3.9-GHz SCRF cavity (CAV39). The 3rd-harmonic cavity will enable the tailoring of nonlinear distortions in the longitudinal phase space (LPS) thereby providing control over the bunch current profile [3]. The beam dynamics performance of the rf photoinjector was reported in Ref. [5]. In this paper we use the latter simulations as a starting point for start-to-end simulations. We restrict our simulations to the case of a photocathode-driven laser with a Gaussian temporal distribution with rms duration $\sigma_t = 3$ ps [4].

Downstream of ACC39, the beamline comprises quadrupole and steerer magnets and a four-bend chicane bunch compressor (BC1 in Fig. 1). The chicane's bends have a nominal bending angles of (+,-,-,+) 18° resulting in a longitudinal dispersion of $R_{56} = -0.19$ m. The longitudinal-phase-space correlation needed to compress the bunch is imparted with CAV2 operating off-crest (and CAV39 at a later stage). Following this 12-m section, the beam is accelerated by a string of three accelerating modules (an ILC accelerating unit; ACC1/2/3 in Fig. 1). Downstream of ACC1/2/3 several options are under consideration. In this paper, we concentrate on an option which could be optimized to produce low-emittance high-peak-current electron bunches for AARD. Such a configuration would incorporate a second-stage bunch compression downstream of ACC1/2/3 and followed by a single accelerating module (ACC4) that would bring the beam's final energy to $\sim$ 900 MeV. The 900-MeV beam could either be directed to a spectrometer line consisting of two dipoles and an achromatic section, or be used for AARD experiments in a high-energy user area consisting of several parallel beamlines.

In this paper we concentrate on a variant of the aforementioned configuration where the CAV39 and the second-stage bunch compressor are absent. In this scenario, the bunch can only be compressed in BC1 and CAV2 is therefore operated off-crest to minimize the bunch length downstream of BC1.

SINGLE-PARTICLE DYNAMICS

The anticipated beam parameters make the beam sensitive to collective effects such as space charge, self-interaction via coherent synchrotron radiation (CSR) and wakefields. Our design tools consist of using the single-particle-dynamics program ELEGANT v.24.1 [6] to optimize the beamline configuration and magnet strengths. Simulations with IMPACT-Z [7] are then performed to explore the effects of space charge. CSR effects are also included in IMPACT-Z but a previous study indicates that the phase space degradation during compression in BC1 is dominated by space charge effects [5].

The quadrupole magnet strengths were determined using ELEGANT built-in fitting routines. The settings of the quadrupole magnets upstream of the bunch compressors are chosen to achieve horizontal waist with small betatron function value between the third and fourth dipoles of the chicanes (a prescription to minimize CSR-induced transverse emittance dilution). The quadrupole-magnet triplet located downstream of BC1 focusses the beam at the loca-

* This work was supported by LANL Laboratory Directed Research and Development (LDRD) program, project 20110067DR and by the U.S. Department of Energy under Contract No. DE-FG02-08ER41532 with Northern Illinois University and under Contract No. DE-AC02-07CH11359 the Fermi Research Alliance, LLC.

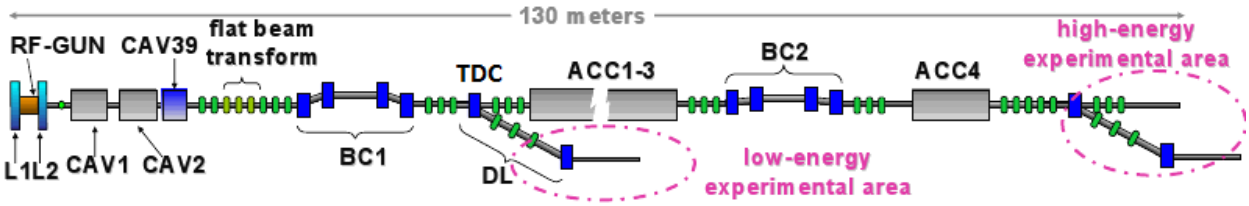

Figure 1: Overview of the beamlines. The legend is "L1" "L2" solenoidal magnetic lenses, "CAV1" "CAV2" superconducting TESLA cavity, "CAV39" third harmonic ($f = 3.9$ GHz) superconducting cavity, "BC" magnetic bunch compressor chicane, "DL" dogleg to low-energy experimental line, "TDC" transverse deflecting cavity. The green rectangles indicate the locations of quadrupoles.

Table 1: Operating parameters of the accelerating modules for the simulations presented in this paper. The accelerating module cavities are assumed to operate with average energy gradient 26 MeV/m.

Parameter	Value	Unit
Peak energy gain in CAV2	22	MeV
off-crest phase CAV2	[-27, -20]	deg
Peak energy gain in ACC1/2/3	645	MeV
off-crest phase ACC1/2/3	0	deg
Peak energy gain in ACC4	215	MeV
off-crest phase ACC4	0	deg
Energy at CAV2 exit	~ 40	MeV
Final energy	~ 900	MeV

tion of the downstream transverse deflecting cavity (TDC). Finally the quadrupole magnets upstream of the accelerating modules ACC1/2/3 are optimized to produce a divergent beam at the entrance of the modules to counteract the cryomodules' RF-focusing and avoid over focussing in the cryomodules [typically ($\alpha_{x,y} \simeq -5$, $\beta_{x,y} \simeq 15$ m)]. The quadrupole magnets upstream of the spectrometer line are tuned to match to the design initial Courant-Snyder parameters for the spectrometer beamline. The spectrometer section consists of an achromatic dogleg followed by a transport line whose prime purpose is to defocus the beam before it hits the dump. The beam's energy and energy spectrum are measured with beam position monitor and transverse density monitor located at two high dispersion points $\eta \simeq 0.55$ m inside the dogleg. The evolution of the betatron function along the 120-m accelerator beamline (starting at $z = 8.54$ m from the photocathode) is depicted in Fig. 2. The betatron functions remain below 100 m in both transverse planes (the large values close to $z \simeq 120$ m correspond to the dump location).

The final magnet settings devised in ELEGANT are then imported into an IMPACT-Z model. The initial distributions tracked in IMPACT-Z are obtained from ASTRA simulations [8] in Ref. [5]. A comparison of the rms beam sizes and mean energy and fractional energy spread simulated in IMPACT-Z and ELEGANT is shown in Fig.3. The longitudinal beam parameters are in excellent agreement while the transverse beam envelope agrees reasonably well along most of the accelerator beamline. We attribute the slight disagreement to differences in the accelerating-cavity models. In IMPACT-Z a cavity is modeled by a Fourier series of the axial accelerating field $E_z(z, r = 0)$ while in ELEGANT the focusing is modeled via an impulse approximation (entrance/exit kick for each cell composing the 9-cell TESLA cavity) along with body focusing described by a linear transfer matrix; see Ref. [9].

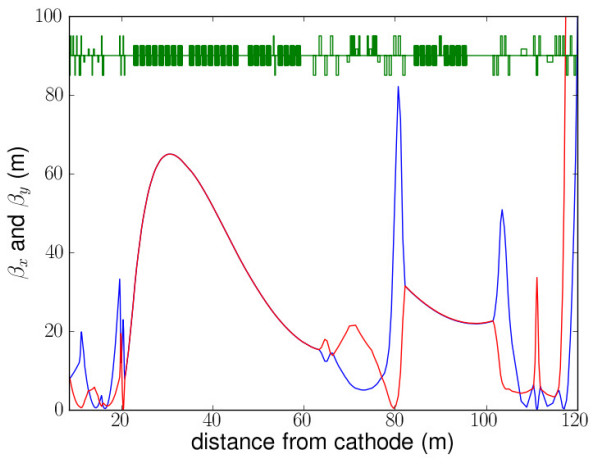

Figure 2: Lattice functions β_x (blue) and β_y (red) along the STF@NML beamline simulated with ELEGANT.

MULTI-PARTICLE DYNAMICS

The multi-particle dynamics simulations were performed with IMPACT-Z using an input distribution produced with ASTRA. The beamline was split into five sections: (i) the injector transport ($8.54 \leq z \leq 21$ m), (ii) the ILC accelerating unit which corresponds to ACC1/2/3 ($21 \leq z \leq 59$ m), (iii) the BC2 section including the upstream and downstream quadrupole magnets ($59 \leq z \leq 83$ m), (iv) the ACC4 accelerating module ($83 \leq z \leq 98$ m), and (v) the spectrometer line and downstream transport to the dump. The tracking through the full beamline

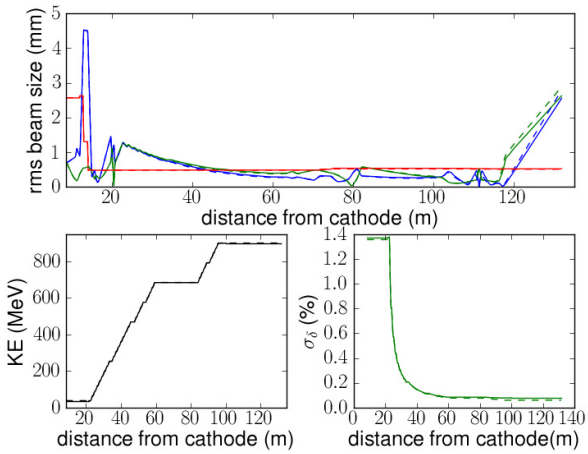

Figure 3: Single-particle-dynamics simulation using ELEGANT (dashed line) and IMPACT-Z showing the evolution of σ_x (blue), σ_y (green) , and σ_z (red) [top plot], the kinetic energy [bottom left] and fractional energy spread σ_δ [bottom right].

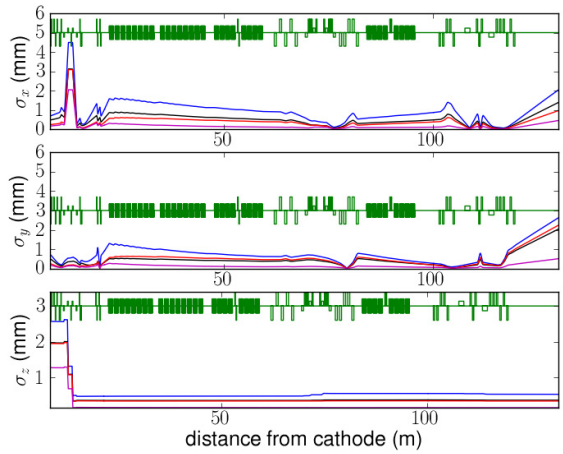

Figure 4: Comparison of horizontal (top) vertical (middle) and longitudinal (bottom) rms beam sizes for bunch charges of 3.2 (blue), 1.0 (black), 0.25 (red), and 0.02 nC (magenta).

Table 2: Transverse emittances and bunchlength upstream and downstream of BC1 (respectively referred with subscripts $_i$ and $_f$) for 4 cases of bunch charges.

Q (nC)	ϵ_{nxi} (μm)	ϵ_{nxf} (μm)	ϵ_{nyi} (μm)	ϵ_{nyf} (μm)	σ_{zi} (mm)	σ_{zf} (mm)
3.2	4.62	13.40	4.61	8.099	2.60	0.53
1.0	2.33	3.393	2.32	2.472	1.97	0.33
0.25	0.598	1.25	0.598	1.392	1.95	0.38
0.02	0.279	0.459	0.279	.366	1.27	0.15

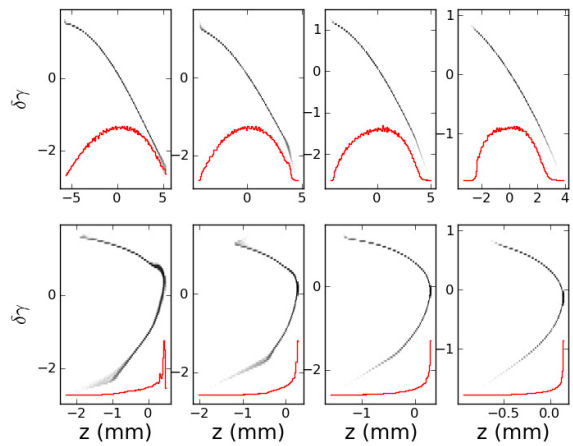

Figure 5: (Top row) LPS distribution upstream (top plots) and downstream (bottom plots) of BC1. The four columns correspond respectively (from left to right) bunch charges of 3.2, 1.0, 0.2, and 0.02 nC. The superimposed white line corresponds to the longitudinal bunch profile. The head of bunch corresponds to $z > 0$.

was automated using GLUETRACK, a PYTHON-based script enabling the integrated simulation of accelerator beamlines [10].

Start-to-end simulations of the beamline were performed for four cases of bunch charges. The beamline was optimized for the 3.2-nC case and the beam distribution corresponding to other charges were numerically matched to the desired Courant-Snyder parameters. The rms beam size evolutions along the beamline appear in Fig. 4 and the LPS distributions before and after BC1 are displayed in Fig. 5. The LPS distribution is strongly distorted by the compression process, resulting in a temporal profile with a local charge concentration in the head of the bunch followed by a long low-charge tail. This nonlinear compression will eventually be corrected with the CAV39.

REFERENCES

[1] J. Liebfritz, et. al, these Proceedings, MOP009. (2011).

[2] see http://projectx.fnal.gov/

[3] K. Flöttmann, et al., TESLA-FEL 2001-06, DESY (2001).

[4] J. Ruan, private communication (2010) .

[5] P. Piot, et al., Proceedings of IPAC'2010, 4316 (2010).

[6] M. Borland, ANL/APS note LS-287 (2000).

[7] J. Qiang, et al., J. Comp. Phys. 163, 434 (2000).

[8] K. Flöttmann, ASTRA *user manual*, DESY (1999).

[9] J. B. Rosenzweig, L. Serafini, Phys. Rev. E 49, 1599 (1994).

[10] I. Zagorodnov, private communication (2010).